Title page

# Radiostrontium sorption on natural glauconite sands of the Neogene-Paleogene formations in Belgium

Y. Bruneel[1,2] , L. Van Laer[1], S. Brassinnes[3], E. Smolders[2]

[1] Belgian Nuclear Research Centre (SCK CEN), Expert Group Waste & Disposal, Boeretang 200, 2400 Mol, Belgium

[2] Department of Earth and Environmental Sciences, Division of Soil and Water Management, KU Leuven, Kasteelpark Arenberg 20, 3001 Leuven, Belgium

[3] ONDRAF/NIRAS, the Belgian Agency for Radioactive Waste and Fissile Materials, Kunstlaan 14, 1210 Brussel, Belgium

Corresponding Author. Contact: yaana.bruneel@sckcen.be

## Highlights

- Radiostrontium retention in Neogene glauconite sands unknown
- $^{90}Sr$ sorption $K_D$ on natural glauconite sands range from 23 to 65 L $kg^{-1}$
- $K_D$ in the glauconite fraction differs with a factor 3
- Sorption equilibrium is reached in all fractions within 48 hours
- $^{90}Sr$ sorption $K_D$ can be well predicted based on the CEC and Ca concentration

## Abstract

The Neogene-Paleogene glauconite sands are investigated for radionuclide sorption in the framework of the Belgian radioactive waste disposal program. This study was set up to measure the adsorption of radiostrontium ($^{85}Sr$) on the sands and on glauconite fractions to identify factors explaining variable sorption among different formations. Batch $^{85}Sr$ sorption experiments were set up with 45 different glauconite sands and glauconite fractions (125-250 µm) in a background solution of 1 mM $CaCl_2.H_2O$ and 0.5 mM KCl. The distribution coefficients ($K_D$) for $^{85}Sr^{2+}$ ranged 23-65 L $kg^{--1}$ for the intact sands and ranged 50-144 L $kg^{-1}$ for the glauconite fractions. The $K_D$ values strongly correlated with the CEC ($R^2$ =0.62 for sands and 0.82 for glauconite fractions) and corresponded well with CEC based predictions based on two existing models calibrated to soils. The $K_D$ on the complete sand is proportional to the glauconite content and the $K_D$ of the glauconite fraction if no other clay minerals are present in significant amounts. Sorption equilibrium was reached within 48 hours in the complete sands, in milled complete sands, in glauconite fractions and in milled glauconite fractions, suggesting no diffusive boundaries in the glauconite pellets. It is concluded that glauconite sands have a suitably high retention of radiostrontium and the sorption strength is in line with that of other geological barriers when judged from the CEC.

## Keywords

Glauconite; Neogene-Paleogene; Strontium; Sorption; Cation Exchange Capacity

# 1 Introduction

Safe storage of radioactive waste for hundreds to hundreds of thousands of years is one of the basic requirements of radioactive waste disposal. To assess the long-term safety of disposal sites, a good understanding of the processes and mechanisms controlling the radionuclide (RN) transport in the various system components is essential. Due to the long residence time of radioactive waste in the disposal site, a natural barrier will need to take over the role of the engineered barrier. In Belgium the Neogene glauconite sands have been considered as an extra embankment below the surface disposal for the short-lived and low-level waste. For the high-level and/or long-lived radioactive waste a geological disposal is proposed. Depending on the chosen host rock, glauconite sand can be present next to the natural barrier, as is the case for the Boom Clay and Ypresian clays.

The glauconite content of the Neogene Diest and Berchem Formation (Fm) varies between 35-40 %, with locally up to 89 % glauconite (e.g. Berchem Fm). The glauconite occurs in the glauconite sands mostly as sand sized pellets. This strongly affects the properties of the sands that logically have high porosities and permeabilities. Glauconite is an iron (Fe) -rich dioctahedral mica, though it can be compared to an Fe-rich illite structure-wise with potassium ($K^+$) the dominant interlayer cation. The mineral glauconite is defined as $K\ (R^{3+}_{1.33}\ R^{2+}_{0.67})\ (Si_{3.67}\ Al_{0.33})\ O_{10}(OH)_2$ with $Fe^{3+}$ >> aluminium ($Al^{3+}$) and magnesium ($Mg^{2+}$) > $Fe^{2+}$. In the tetrahedral positions $Al^{3+}$ or $Fe^{3+}$ occupy more than 0.2 atoms per formula unit with the trivalent cations ($R^{3+}$) > 1.2 atoms per formula unit. Finding a pure glauconite is exceptional, most often glauconite pellets consist of one or more mixed layer glauconite-smectite phases (Adriaens et al., 2014; Meunier and El Albani, 2007). The diverse composition of glauconite pellets, even in similar formations, stems from both the formation and weathering history. Glauconite is a redox sensitive mineral due to the presence of both $Fe^{3+}$ and $Fe^{2+}$. Weathering affects the cation composition of the structure. Iron and $Mg^{2+}$ are removed or substituted in the structure and $K^+$ is leached from the interlayer (Courbe et al., 1981; Van Ranst and De Coninck, 1983).

Radiostrontium ($^{90}Sr$) is as a fission product of uranium and plutonium present in nuclear waste and in sites contaminated by nuclear accidents. The radionuclide (RN) has a half-life of 28.78 years and is highly soluble under all $E_h$ and pH conditions occurring as the divalent cation $Sr^{2+}$. Strontium sorption depends on the cation exchange capacity (CEC) of the solid phase, the ionic strength and the pH (Bradbury and Baeyens, 2005; Wallace et al., 2012). The solid-liquid distribution coefficient $K_D$ of $^{90}Sr$ is well below that of $^{137}Cs$. The $Sr^{2+}$ log $K_D$ on illite is 1.9 ± 0.3 with the $K_D$ expressed in L $kg^{-1}$ at 0.1 M ionic strength and pH 7 (Altmann et al., 2014; Poinssot et al., 1999). As the ionic strength decreases to 0.01 M, the log $K_D$ increases with 1 to 1.5 units (Altmann et al., 2014) or even 2 units (Poinssot et al., 1999) in the pH range 5.5 to 8.3. For pure glauconite, log $K_D$ for Sr is 1.9 ± 0.2 L $kg^{-1}$ in tap water with pH 7.8 at 0.1 mM $K^+$, 1.1 mM $Na^+$, 1 mM $Ca^{2+}$, 0.3 mM $Mg^{2+}$(Voronina et al., 2015).

The uptake of $Sr^{2+}$ on glauconite is expected to be dominated by cation exchange processes similar to $Sr^{2+}$ sorption on illite. Strontium is predominantly bound by outer sphere bonding on the planar sorption sites making it vulnerable to exchange by cations with higher charge density. The capacity of the planar sites is reflected in the effective CEC, i.e. the CEC valid at the pH at which the sorption is measured. For illite a large variation in the capacity of the planar sites is found in literature, ranging from 80 to 98% of the CEC (Bradbury and Baeyens, 2000; Brouwer et al., 1982; Fuller et al., 2014; Missana et al., 2014). In smectite minerals the fraction of planar sites increases to nearly 100 % of the CEC. Contrary to illite, the interlayer is accessible to (hydrated exchangeable) cations in smectite like minerals. Glauconite occurs mostly as a mixed layer mineral of illite-like and smectite-like end members (Meunier and El Albani, 2007). The CEC of illite ranges 20-40 cmolc $kg^{-1}$, that of smectite 80-120 $cmol_c$ $kg^{-1}$ (Meunier, 2005) and the selected data for glauconite indicate an intermediate CEC suggesting that the $K_D$ of $Sr^{2+}$ is between that of illite and that

of smectite. The $Sr^{2+}$ $K_D$ (in L $kg^{-1}$) can be modelled (Eqn. 1) using the selectivity coefficient $K_c$ (Sr/Ca) and the measured effective CEC (eCEC, in mol $kg^{-1}$), if the $Ca^{2+}$ concentration in solution is known and the sorption sites are fully occupied with $Ca^{2+}$ (Konoplev et al., 1992; Valcke et al., 1998):

$$K_D = \frac{K_c(Sr/Ca) \cdot CEC \cdot Z_{Ca}}{2\, m_{Ca}} \quad (1)$$

With $Z_{Ca}$ the fractional loading of $Ca^{2+}$ on the sorption sites and $m_{Ca}$ the concentration of $Ca^{2+}$ in solution in mol $L^{-1}$.

A high ionic strength is measured at many nuclear legacy sites, versus low ionic strength in the natural pore waters of the potential glauconite sand to RN interaction. At neutral pH, $Ca^{2+}$ and $Mg^{2+}$ in solution will compete with $Sr^{2+}$ and the distribution ratio's in the background electrolyte will determine the sorption of each cation (Poinssot et al., 1999). In acid environments the permanently negatively charged surfaces will become protonated and hydrogen ($H^+$) will compete with the cations in solution for the sorption sites. However, at low pH the clay can start to dissolve, releasing cations in solution and giving rise to secondary precipitation. Below pH 5.5 Poinssot et al. (1999) observed a decrease in $Sr^{2+}$ sorption combined with an increase of cations in solution due to partial dissolution of the clay. In the pH range 5.5 to 8.5 the sorption remains relatively stable, above pH 8.5 an increase in $Sr^{2+}$ sorption can be observed possibly due to surface complexation reactions similar to $Ca^{2+}$ sorption on Na-montmorillonite (Baeyens and Bradbury, 1995; Poinssot et al., 1999).

This study aimed to assess the sorption of radiostrontium on natural glauconite sands from the Neogene-Paleogene formations in Belgium and to identify the factors explaining the variation in $Sr^{2+}$ sorption among the samples (n=45 sand samples). The effect of glauconite weathering on Sr sorption was evaluated by comparing a range of naturally weathered glauconite sands with subsurface samples. The role of sorption kinetics and of diffusion within glauconite pellets was addressed by measuring adsorption kinetics on glauconite fractions that were either or not milled before the adsorption tests. Recent studies with $^{137}Cs$ sorption on equivalent substrates identified such diffusive boundaries (Bruneel et al., 2020).

# 2 Materials and methods

## 2.1 Natural glauconite sands

Natural glauconite sands occur in the Neogene and Paleogene formations mainly situated in the North and North-East of Belgium. For the surface disposal the Neogene Berchem and Diest Formation are of importance, though the Paleogene Voort and Eigenbilzen Formation can give additional information on the additional natural barrier for a possible repository in the Boom Clay. The glauconite in the investigated formations is very diverse in grain size, morphology and colour (Bruneel et al., 2020).

### 2.1.1 Voort Fm

The Voort Formation is Paleogene in age (Chattian 28.1 – 23 Ma) and forms the transition to the Neogene sands from the Eigenbilzen and Boom Clay Formation. The Voort Formation is a fine grained and clay rich sand characterised by a high glauconite content. Disperse clay layers are present reducing the permeability of the formation. The transition to lower Eigenbilzen Fm and Berchem Fm above are gradual (Adriaens et al., 2014).

### 2.1.2 Berchem Fm

The Berchem Formation consists of three members, Edegem, Kiel and Antwerp, separated by hiatal intervals as the result of deposition in marginal marine environments with fluctuating sea levels (Adriaens et al., 2014; Vandenberghe, 2004). The lithology is characterised by highly glauconitic sands with frequent clay intercalations. The three members are fine- to medium-grained sand units and distinction among them is made based on the calcareous fossils, dinoflagellate biozonations and glauconite content (Louwye, 1999; Louwye et al., 2006). Due to the marginal marine conditions not all members of the Berchem Formation have been deposited over the total Campine area. In the region of Mol – Dessel only the Antwerp Member is present. It is characterised by a high glauconite content of about 46 % with local units enriched in glauconite up to 70-80 %. The glauconite pellets are described as smectite rich high expandable glauconite-smectite. Towards the underlying Voort Formation the Antwerp Member becomes more clay rich and more fine grained. The mineralogy of the disperse clay layers in the Antwerp Member were characterised by Adriaens (2015) and contains no glauconite.

### 2.1.3 Diest Fm

Sedimentation only restarted after an important phase of erosion known as the Mid-Miocene unconformity. Due to the erosion phase the Diest Fm has a highly irregular base with gully structures to go up to the Boom Clay Formation in some locations. The Diest Fm itself is characterised by poorly sorted, coarse glauconitic sands with low clay fraction content. The Diest Formation was deposited over a larger region giving rise to lateral variation (Adriaens et al., 2014; Louwye, 1999; Louwye and De Schepper, 2010; Louwye et al., 2006). The lower Diest formation is defined as the Dessel member in the Dessel-Mol region. This lower member has 26 % glauconite described as smectite rich high-expandable glauconite smectite. The upper Diest formation is more coarse and has glauconite contents of about 38 % characterised as glauconite-smectite low-expandable (Adriaens et al., 2014).

### 2.1.4 Naturally weathered glauconite sands

Due to a dip to the east, the Neogene formations have outcrops at the surface (Figure 1). For this study a set of subsurface samples (from drilling cores) and surface samples (collected in quarries and outcrops) was selected (Table1). The subsurface samples represent the glauconite sands in its current state. Subsurface samples were selected from the Kasterlee Fm, Diest Fm, Berchem Fm and Voort Fm. The surface samples are subjected to the elements in natural outcrops and quarries. These naturally weathered samples were selected to test the effect of weathering of the glauconite sands on the sorption

of Sr. Samples of the weathered Diest Formation sands were collected in Wezemaal, at the Wijngaardberg and Beniksberg, and in Lubbeek in the Zavelstraat. At the Wienerberger quarry in Rumst samples were taken from the green sands above the Boom Clay, part of the Berchem Formation.

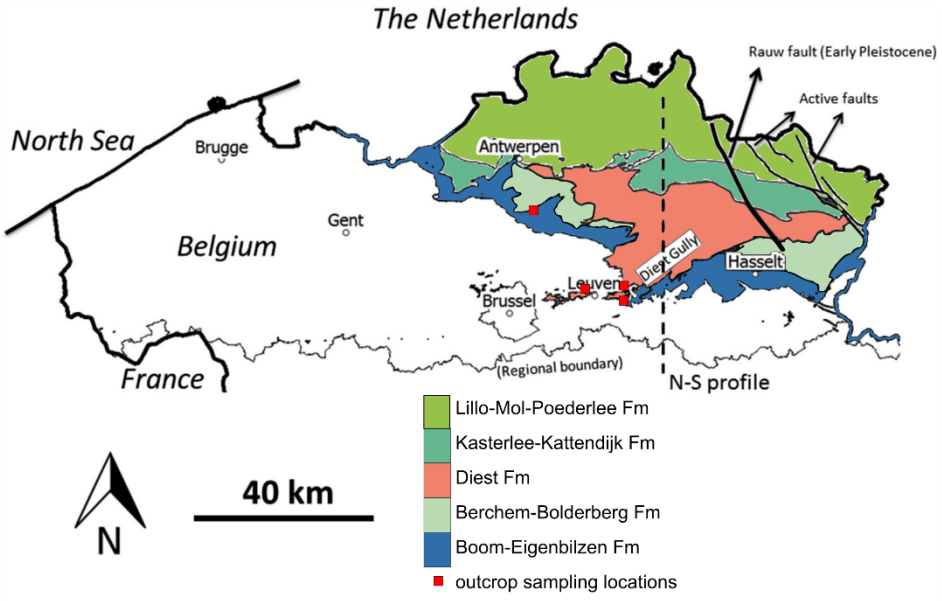


*Figure 1 Outcrop of the Neogene formations in Belgium with indicated sampling locations of the surface sands. Map modified after ALBON (2009).*

*Table 1 Inventory of the selected glauconite sand samples from the Neogene-Paleogene formations for this study. Subsurface samples are indicated with K, D, B or V (indicating the formation Kasterlee, Diest, Berchem or Voort) and originate from the collection of NIRAS/ONDRAF (ON-Mol1 31W237, ON-Dessel3 31W354, ON-Dessel5 31W370 borehole). The samples indicated with shaft excavation originate from the excavation of the second shaft to the underground lab HADES in Mol. Surface samples were collected in Wezemaal, at the Wijngaard or Beniksberg, in Lubbeek in the Zavelstraat and in Rumst at the Wienerberger quarry. The Boom Clay sample is a sample from a recent sampling campaign at HADES level*

| Sample name | Formation | Origin | m TAW[$] | Lithology | Sample fractions | | | |
|---|---|---|---|---|---|---|---|---|
| | | | | | Complete sample | Glauconite fraction | Milled complete sand | Milled glauconite fraction |
| K1 | Kasterlee | ON-Dessel 3-20 | 3.6 | Sand | X | | | |
| D1 | Diest | Shaft excavation | -73 | Sand | X | X | X | X |
| D2 | Diest | Shaft excavation | -91 | Sand | X | X | | |
| D3 | Diest | ON-Dessel 5-30 | -95 | Sand | X | X | X | |
| D4 | Diest | ON-Dessel 5-44 | -109 | Sand | X | X | X | X |
| D5 | Diest | ON-Dessel 5-48 | -113 | Sand | X | X | X | X |
| D6 | Diest | Shaft excavation | -78 | Sand | X | X | X | |
| D7 | Diest | Shaft excavation | -83 | Sand | X | | | |
| D8 | Diest | ON-Dessel 5-20 | -85 | Sand | | X | | X |
| D9 | Diest | Shaft excavation | -101 | Sand | X | X | | |
| D10 | Diest | ON-Dessel 5-44 | -109 | Sand | | X | | |
| D11 | Diest | Boring Put 8_PIDPA | -48 | Sand | | X | | X |
| D12 | Diest | Boring Put 8_PIDPA | -52 | Sand | | X | | |
| D13 | Diest | Boring Put 8_PIDPA | -60 | Sand | | X | | |
| D14 | Diest | Boring Put 8_PIDPA | -96 | Sand | | X | | X |
| D15 | Diest | Boring Put 8_PIDPA | -104 | Sand | | X | | |
| D16 | Diest | Boring Put 8_PIDPA | -108 | Sand | | X | | |
| B1 | Berchem | ON-Dessel 5-63 | -126 | Sand | X | X | X | X |
| B2 | Berchem | Shaft excavation | -134 | Sand | X | X | X | X |
| B3 | Berchem | ON-Mol 1-14 | -134 | Sand | X | | | |
| B4 | Berchem | ON-Dessel 5-77 | -140 | Sand | | X | | |
| V1 | Voort | Shaft excavation | -144 | Clayey sand | X | X | X | X |
| V2 | Voort | Shaft excavation | -152 | Clayey sand | X | | | |

| | | | | | | | |
|---|---|---|---|---|---|---|---|
| V3 | Voort | Shaft excavation | -140 | Clayey sand | X | X | |
| V4 | Voort | ON-Mol 1-24 | -144 | Clayey sand | X | | |
| V5 | Voort | Shaft excavation | -141 | Clayey sand | X | | |
| V6 | Voort | Shaft excavation | -147 | Clayey sand | | X | |
| W1 | Diest | Wijngaardberg, Wezemaal | 55 | Sand | X | X | |
| W2 | Diest | Wijngaardberg, Wezemaal | 55 | Sand | X | X | |
| W3 | Diest | Wijngaardberg, Wezemaal | 51 | Sand | X | | |
| W4 | Diest | Wijngaardberg, Wezemaal | 51 | Sand | X | X | |
| W5 | Diest | Beniksberg, Wezemaal | 44 | Sand | X | X | |
| W6 | Diest | Beniksberg, Wezemaal | 44 | Sand | X | X | |
| W7 | Diest | Beniksberg, Wezemaal | 45 | Sand | X | X | |
| W8 | Diest | Beniksberg, Wezemaal | 45 | Sand | X | X | |
| W9 | Diest | Beniksberg, Wezemaal | 45 | Sand | X | X | X |
| W10 | Diest | Zavelstraat, Lubbeek | 56 | Sand | X | X | |
| W11 | Diest | Zavelstraat, Lubbeek | 56 | Sand | X | X | X |
| W12 | Berchem | Wienerberger, Rumst | 26 | Sand | X | X | |
| W13 | Berchem | Wienerberger, Rumst | 26 | Sand | X | X | |
| W14 | Berchem | Wienerberger Rumst | 31 | Sand | X | X | |
| W15 | Berchem | Wienerberger, Rumst | 27 | Sand | X | X | |
| W16 | Berchem | Wienerberger, Rumst | 27 | Sand | X | X | |
| W17 | Berchem | Wienerberger, Rumst | 26 | Sand | X | X | |
| W18 | Berchem | Wienerberger, Rumst | 28 | Sand | X | X | |
| I | Na-illite du Puy | Reference material | | Clay | X | | |
| BC | Boom Clay | HADES sampling campaign 2017 | -197 | Clay | X | | |

*$The sampling depth is expressed in mTAW, or the reference level in Belgium (Tweede Algemene Waterpassing).*

## 2.2 Sample preparation

For analysis and batch sorption studies, four different fractions of the glauconite sands were prepared, i.e. the complete sand, the glauconite fraction, the milled complete sand and the milled glauconite fraction. For a selection of the samples (selected from the collection of R. Adriaens), only the glauconite fractions were available (D8, D10-16 and B4). These four fractions were prepared for several reasons. The glauconite content is variable over the glauconite sand formations. By separating the glauconite fraction from the matrix the effect of the glauconite mineral and chemical variability on $Sr^{2+}$ sorption can be tested. Radiocesium sorption on the glauconite sands (Bruneel et al., 2020) revealed a strong effect of the particle size on the sorption kinetics and restricted access to the sorption sites at the centre of the grain. To make all sorption sites accessible for comparison, milled complete glauconite sands and milled glauconite fractions were prepared.

The complete sands required only drying (oven drying at 60 °C). To separate the glauconite fraction, the complete sands were wet sieved to obtain the 125-250 µm size fraction. This is the dominant size fraction in the sands and has sufficiently large glauconite grains to allow good separation of the glauconite fraction from the quartz phases by magnetic separation. The oven dried (60 °C) glauconite fraction was separated using a Frantz isodynamic magnetic separator. The milled fractions were produced with a McCrone Micronizing mill using zirconium grinding elements. The samples were wet milled with ethanol to avoid amorphisation of the crystal structure.

## 2.3 Sample analysis

A smaller set of samples was analysed in more detail to relate Sr sorption to mineral or chemical parameters of the glauconite sands and fractions.

Powder X-ray diffraction (XRD) analysis was used to determine the glauconite content, the total clay content and position of the $d_{060}$ reflection and was applied to 29 samples. The glauconite sands were milled (McCrone) with zincite as internal standard (for quantification 10 wt % zincite, for $d_{060}$ determination 5 wt % zincite). To avoid preferred orientation, the samples were side loaded in the sample holders. Data interpretation and quantitative data analysis was done using QUANTA (© Chevron ETC). The $d_{060}$ reflection allows the distinction between dioctahedral and trioctahedral clay minerals and is sensitive to weathering. The reflection depends on the size of the cations and the cation occupancy in the octahedral layer (Moore and Reynolds, 1997).

The cation exchange capacity (CEC) at the pH of the substrate was determined using a cobalt (III) hexamine chloride cation exchange (standardized protocol ISO 23470 (2007)). All samples were milled before CEC determination. The glauconite grains or pellets are relatively large (125-250 µm average) and not all of the internal cation exchange sites are instantly accessible to the large cobalt(III) hexamine cation. The standard protocol for the CEC determination uses one hour equilibration time, therefore milling was used. Using longer equilibration times might overcome diffusion limitation in the kinetics of the cation exchange reaction. On a subset of samples, both milled and un-milled, the cobalt (III) hexamine chloride cation exchange was extended to 14 days with regular samples. In addition, CEC was also determined on five non-milled samples.

The elemental composition was determined on nine complete glauconite sands and glauconite fractions. To the batch, a set of six reference samples were added (BCR-2, MRG-1, BCS-267, BCS-269, NIST-610, GA). The samples were prepared in duplicate with the lithium(Li)-metaborate fusion method of Vassilieva

modified from Suhr and Ingamells (1966) and Cremer and Schlocker (1976). The samples were measured with Inductively Coupled Plasma Optical Emission Spectroscopy (ICP-OES – Varian 720ES).

The speciation of $Fe^{2+}$ to $Fe^{3+}$ in the glauconite fraction was determined on 31 samples using the 1.10-phenantroline method (Shapiro 1960, Fritz et al. 1985). The phenantroline forms a bright orange complex with $Fe^{2+}$ and prevents further oxidation. The $Fe^{2+}$ content can be determined based on the UV-VIS absorbance in the supernatants at 555 nm (Varian Model 635 UV-Visible Spectrometer). The total Fe content of the supernatants was determined at 248 nm by Atomic Absorption Spectroscopy (AAS) (Thermo Electron Corporation S series AAS). The $Fe^{2+}$ and $Fe_{tot}$ mass percentages are calculated through a calibration curve obtained from geological Standard Reference Materials (SRM). A set of seven SRM's with similar $Fe^{2+}$ and $Fe_{tot}$ contents to the glauconite fraction were added to the batch (NIM-G, GA, SY-3, DR-N, MRG1, BCR1 and NIM-D), all analyses were performed in triplicate.

## 2.4 Batch sorption studies

The Sr batch sorption experiment was performed in a background solution of 1 mM $CaCl_2.H_2O$ and 0.5 mM KCl (I=0.002 M) with a solid liquid ratio of 1 g to 30 mL. The background concentration was chosen to be representative of the in-situ pore water in the Neogene-Paleogene formations (0.14-0.37 mM $K^+$ and 0.3-1.7 mM $Ca^{2+}$). The experiment was performed in duplicate and with $^{85}Sr$ as an analogue for $^{90}Sr$. To ensure equilibrium between the sample and the background solution, the background solution was changed four times over the course of three days prior to Sr addition. A dialysis membrane (MWCO 6-8 kD) was used to contain the sample and 5 mL solution and prevent loss of the fine fraction during solution changes. After equilibration, the supernatant was spiked with $^{85}Sr$ and initial activities in all samples were 310 Bq $mL^{-1}$. The suspensions were equilibrated in an end-over-end shaker (0.42 $s^{-1}$) at 25°C and the solution was sampled after 48 hours, 7 days, 14 days, 28 days and 56 days. The activity in solution was analysed using a gamma counter and all activity concentrations were decay corrected. The distribution coefficient of $^{85}Sr$ ($K_D$) between the sorbed activity and activity in solution is used to express the sorption of radiostrontium on glauconite (sands).

$$K_D = \frac{A_{ini} - A_{eq}}{A_{eq}} \cdot \frac{V}{m} \qquad (2)$$

with $A_{ini}$ and $A_{eq}$ the initial and equilibrium activity in solution, with $V$ the solution volume (L) and $m$ the sample mass (kg).

# 3 Results

## 3.1 Radiostrontium sorption on glauconite sands

The adsorption kinetics showed that the $K_D$ values beyond 48 h and up 56 days ranged factors 0.85-1.1 of the corresponding values at 48 h, illustrating that sorption equilibrium was reached after 48 h in all fractions data not shown). The complete sand and glauconite fraction were milled to test the accessibility of the sorption sites in the glauconite pellets. After 48 hours, the $K_D$ of the milled and intact complete sands was almost identical, the ratio of the $K_D$ of the milled to that of the intact complete sand ranged 0.97 to 1.13. Similar ratios are observed between the milled glauconite fraction and the intact glauconite (0.88 to 1.50). Taken together, that data shows that slow reactions related to micropore diffusion in the pellets are negligibly small.

The distribution coefficients of $Sr^{2+}$ sorption after 48 h on the four different fractions of the glauconite sands are summarised in Table 2. The measurement error between two replicates, expressed as standard deviation/mean was 7.4 % on average, illustrating a rather high precision. The $K_D$ values (± standard deviation) for the Neogene and Paleogene glauconite sands range between 23 and 65 L $kg^{-1}$ for CEC values ranging between 8.3 and 15.4 $cmol_C$ $kg^{-1}$. The CEC values for the glauconite fractions range between 20.7 and 33.6 $cmol_C$ $kg^{-1}$, higher than reported for the Illite du Puy references (20 $cmol_C$ $kg^{-1}$) (Bradbury and Baeyens, 2000). For the internal reference sample Illite du Puy, a $K_D$ of 132 L $kg^{-1}$ was measured, while the $K_D$ values range between 50 and 144 L $kg^{-1}$.This means that lower $K_D$ values per unit of CEC are observed for the glauconite sands (2.3-5.0, mean 3.8 L $kg^{-1}$/($cmol_c$ $kg^{-1}$)) than for illite (6.1 L $kg^{-1}$/($cmol_c$ $kg^{-1}$)). The Sr sorption in the complete sand is proportional to the glauconite content of the sand, since the CEC of the sands is defined almost completely by the glauconite.

*Table 2 Distribution coefficients of Sr ($K_D$ L $kg^{-1}$) after 48 hours (in a 0.5 mM KCl and 10 mM $CaCl_2.H_2O$ background solution) for the four different fractions of the glauconite sands: the complete sand, the glauconite fraction (GL), the milled complete sand and the milled glauconite fraction. The $K_D$ values are given as means ± standard deviation of two replicates. The average $K_D$ of the complete glauconite sand in each formation was added. The sorption data are complemented by the glauconite content and the cation exchange capacity (CEC) of the complete sand and the glauconite fraction ($cmol_c$ $kg^{-1}$) and the calculated selectivity coefficient ($K_c$ (Sr/Ca)). * The measured CEC value for Na-illite du Puy, within the expected range compared to literature references (20 cmolc kg-1 (Bradbury and Baeyens, 2000)).*

| | Sand | Fm average | Milled sand | GL | Milled GL | GL content | CEC Sand | CEC GL | $K_c$ (Sr/Ca) |
|---|---|---|---|---|---|---|---|---|---|
| | | | $K_D$ L $kg^{-1}$ | | | wt % | $cmol_c$ $kg^{-1}$ | | |
| K1 | 6 ± 0.1 | | | | | 3 | 3.6 | | 1.7 |
| D1 | 51 ± 2.4 | 41.6 ± 9.8 | 53 ± 0.5 | 116 ± 0.7 | 130 ± 0.1 | 34 | 10.7 | 26.9 | 4.8 |
| D2 | 37 ± 11 | | | 89 ± 0.1 | | 27 | 8.2 | 24.2 | 4.5 |
| D3 | 35 ± 3.5 | | 41 ± 0.5 | 121 ± 1.2 | | 24 | 9.4 | 28.8 | 3.7 |
| D4 | 35 ± 0.9 | | 39 ± 0.5 | 131 ± 0.3 | 154 ± 0.2 | 23 | 9.5 | | 3.7 |
| D5 | 58 ± 0.1 | | 56 ± 1.3 | 144 ± 3.6 | 177 ± 3.3 | 30 | 12.0 | 30.1 | 4.9 |
| D6 | 33 ± 14 | | 54 ± 0.5 | 121 ± 0.6 | | 33 | 12.5 | | 2.6 |
| D7 | 53 ± 0.8 | | | | | 30 | 13.1 | | 4.0 |
| D8 | | | | 113 ± 0.3 | 120 ± 2.5 | 23 | | | |
| D9 | 33 ± 0.3 | | | 136 ± 0.1 | | 18 | 10.4 | 33.1 | 3.1 |
| D10 | | | | 132 ± 0.4 | | 31 | | 33.6 | 3.9 |
| D11 | | | | 50 ± 0.3 | 75 ± 1.5 | 43 | | 20.7 | 2.4 |
| D12 | | | | 71 ± 0.1 | | 40 | | 21.9 | 3.2 |
| D13 | | | | 81 ± 0.1 | | 41 | | 23.9 | |
| D14 | | | | 107 ± 0.4 | 130 ± 27 | 44 | | | 3.4 |
| D15 | | | | 91 ± 0.5 | | 43 | | 26.0 | 3.5 |
| D16 | | | | 101 ± 1.1 | | 40 | | 26.0 | 3.9 |
| B1 | 86 ± 2.0 | 55.8 ± 22 | 85 ± 0.1 | 100 ± 3.0 | 106 ± 0.3 | 89 | 17.4 | 24.8 | 4.9 |
| B2 | 48 ± 4.1 | | 49 ± 0.4 | 139 ± 0.3 | 123 ± 1.0 | 27 | 11.3 | 33.3 | 4.3 |
| B3 | 33 ± 14 | | | | | 15 | 11.0 | | 3.0 |
| B4 | | | | 135 ± 2.4 | | 45 | | 33.1 | 4.1 |

| | | | | | | | | |
|---|---|---|---|---|---|---|---|---|
| V1 | 37 ± 7.6 | 50.1 ± 8.8 | 42 ± 0.2 | 126 ± 0.5 | 17 | 11.1 | | 3.4 |
| V2 | 47 ± 0.6 | | | | 8 | 11.3 | | 4.2 |
| V3 | 50 ± 1.1 | | | 141 ± 0.7 | 17 | 13.8 | | 3.6 |
| V4 | 65 ± 3.0 | | | | 37 | 12.9 | | 5.0 |
| V5 | 51 ± 0.1 | | | | 16 | 15.4 | | 3.3 |
| V6 | | | | 143 ± 1.8 | 16 | | | |
| W1 | 49 ± 3.2 | 43.6 ± 10 | | 112 ± 0.0 | 45 | 11.3 | | 4.3 |
| W2 | 31 ± 0.4 | | | 64 ± 0.3 | 33 | 9.1 | 24.1 | 3.4 |
| W3 | 56 ± 4.4 | | | | 47 | 12.0 | | 4.7 |
| W4 | 51 ± 0.5 | | | 119 ± 4.3 | 37 | 11.2 | | 4.6 |
| W5 | 39 ± 0.4 | | | 86 ± 0.7 | 40 | 10.4 | | 3.8 |
| W6 | 36 ± 1.3 | | | 108 ± 4.8 | 29 | 12.2 | | 2.9 |
| W7 | 44 ± 0.9 | | | 114 ± 1.8 | 35 | 11.5 | | 3.8 |
| W8 | 40 ± 0.2 | | | 80 ± 0.7 | 40 | 10.9 | | 3.7 |
| W9 | 36 ± 0.5 | | 40 ± 1.1 | 78 ± 1.7 | 39 | 14.1 | | 2.5 |
| W10 | 55 ± 0.5 | | | 99 ± 2.6 | 49 | 13.8 | | 4.0 |
| W11 | 49 ± 0.3 | | 52 ± 0.5 | 81 ± 0.9 | 43 | 12.3 | | 4.0 |
| W12 | 33 ± 0.1 | | | 84 ± 0.9 | | 9.7 | | 3.4 |
| W13 | 56 ± 5.4 | | | 118 ± 0.4 | | 15.3 | | 3.7 |
| W14 | 52 ± 4.5 | | | 120 ± 1.1 | | 15.0 | | 3.5 |
| W15 | 32 ± 14 | | | 73 ± 0.8 | | 9.0 | 28.6 | 3.5 |
| W16 | 23 ± 3.7 | | | 70 ± 0.2 | | 10.2 | | 2.3 |
| W17 | 57 ± 0.5 | | | 129 ± 15 | | 13.1 | | 4.4 |
| W18 | 45 ± 0.1 | | | 124 ± 0.4 | | 13.1 | | 3.4 |
| I | 132 ± 3.2 | | | | | 20.4* | | 6.1 |
| BC | 70 ± 2.3 | | | | | 24.0 | | 2.9 |

## 3.2 Properties affecting the Sr sorption

The correlation analysis (Table 4) suggests that several parameters are indicative for the Sr sorption $K_D$ (after 48 h) in the complete glauconite sands; the CEC (r 0.95, p <0.001), the glauconite content (r 0.69, p <0.001 ) and the total clay content (r 0.81, p <0.001 ). The CEC provides the best prediction of $K_D$ values (Figure 2). Glauconite is the major cation exchanging component in the sand and the most important component of the clay fraction. Only in the Voort Fm samples, the content of other clays (smectite, illite, chlorite) increases and the glauconite fraction alone provides an underestimate of the $K_D$ value of the complete sand.

The Neogene-Paleogene glauconite sands are very diverse in glauconite content, grain size of the glauconite, morphology and the grade of exterior weathering. The diversity is assessed by the major element composition, content of the bulk composition (XRD) and the iron speciation. Glauconite has both $Fe^{2+}$ and $Fe^{3+}$ in the structure and is redox sensitive. It is expected that this ratio will change during weathering. The major element content of the complete sands and the glauconite fraction and the iron speciation in the glauconite fraction are given in Tables 2&3.

*Table 3 Results of the major element analysis and iron speciation in the complete glauconite sands and glauconite fraction.*

| | | |
|---|---|---|
| | Major elements | |
| Sand | Al | 2.2-4.6 wt% |
| | K | 2.3-5.9 wt% |
| | Mg | 0.60-2.0 wt% |
| | Fe | 2.6-15.2 wt% |
| Glauconite fraction | Al | 3.6-5.2 wt% |
| | K | 4.8-7.0 wt% |
| | Mg | 1.8-2.3 wt% |
| | Fe | 14.1-19.5 wt% |
| | Iron speciation | |
| Subsurface sands | $Fe^{2+}/Fe_{tot}$ | 0.10-0.29 |
| Surface sands | | 0.02-0.17 |

The subsurface samples were compared with the weathered surface samples. Clear signs of weathering are the lower $Fe^{2+}/Fe_{tot}$ ratio's combined with higher total Fe content in the glauconite fraction, due to iron oxides formation. The mean $Fe^{2+}/Fe_{tot}$ of weathered samples was 0.053 whereas this was 0.14 for subsurface samples ($p<0.001$, two sided t-test), the differences in total Fe (16.3 versus 13.3 for weathered versus subsurface) were smaller and less pronounced ($p<0.01$). Weathered intact sand samples had similar CEC and lower $^{85}Sr$ $K_D$ values than corresponding values for the subsurface sands, the ratio of means were only 1.03 (CEC) and 0.84 ($K_D$). However, slight differences in glauconite content between both groups explained these differences since multivariate analysis showed no differences ($p>0.05$) in either CEC and $^{85}Sr$ $K_D$ values between weathered and subsurface samples after correcting for % glauconite in a linear model (details not shown).

*Table 4 The correlation coefficients (r) among the properties of the complete sands and their glauconite fractions. (Significant correlations in bold, ***p <0.001, ** p <0.01, * p <0.05).*

| | | | | | | Complete sand | | | | Glauconite fraction | | | | | |
|---|---|---|---|---|---|---|---|---|---|---|---|---|---|---|---|
| $K_D$ | CEC | GL % | Clay % | $d_{060}$ | $Fe^{2+}$ $Fe_{tot}$ | Al | Fe | K | Mg | Al | Fe | K | Mg | | |
| 1 | **0.94*** ** | **0.69** ** | **0.81**** | -0.18 | 0.12 | 0.03 | 0.12 | 0.15 | 0.14 | -0.02 | 0.01 | 0.20 | 0.17 | $K_D$ | |
| | 1 | 0.56 | **0.72*** ** | -0.03 | 0.17 | 0.11 | 0.23 | 0.24 | 0.23 | -0.19 | 0.29 | 0.36 | 0.22 | CEC | |
| | | 1 | **0.94*** ** | 0.27 | -0.43 | 0.23 | **0.99*** ** | **0.96*** ** | **0.96*** ** | -0.24 | 0.33 | 0.53 | 0.07 | GL% | |
| | | | 1 | 0.09 | -0.29 | 0.46 | **0.94*** ** | **0.99*** ** | **0.99*** ** | -0.15 | 0.26 | 0.50 | 0.14 | Clay % | |
| | | | | 1 | 0.04 | **-0.68** ** | 0.36 | 0.03 | 0.09 | -0.18 | 0.28 | -0.34 | **-0.84*** ** | $d_{060}$ | |
| | | | | | 1 | -0.15 | -0.22 | -0.39 | -0.38 | 0.13 | 0.30 | -0.37 | -0.43 | $Fe^{2+}$ $Fe_{tot}$ | |
| | | | | | | 1 | 0.40 | **0.66** ** | **0.62** ** | -0.10 | 0.12 | **0.56*** | **0.53*** | Al | Sand |
| | | | | | | | 1 | **0.93*** ** | **0.95*** ** | -0.14 | 0.32 | 0.39 | -0.07 | Fe | |
| | | | | | | | | 1 | **0.99*** ** | -0.14 | 0.22 | **0.57*** | 0.23 | K | |
| | | | | | | | | | 1 | -0.06 | 0.17 | **0.49*** | 0.19 | Mg | |
| | | | | | | | | | | 1 | **-0.65** ** | **-0.52*** | 0.10 | Al | GL |
| | | | | | | | | | | | 1 | **0.59*** | 0.03 | Fe | |
| | | | | | | | | | | | | 1 | **0.69** ** | K | |
| | | | | | | | | | | | | | 1 | Mg | |

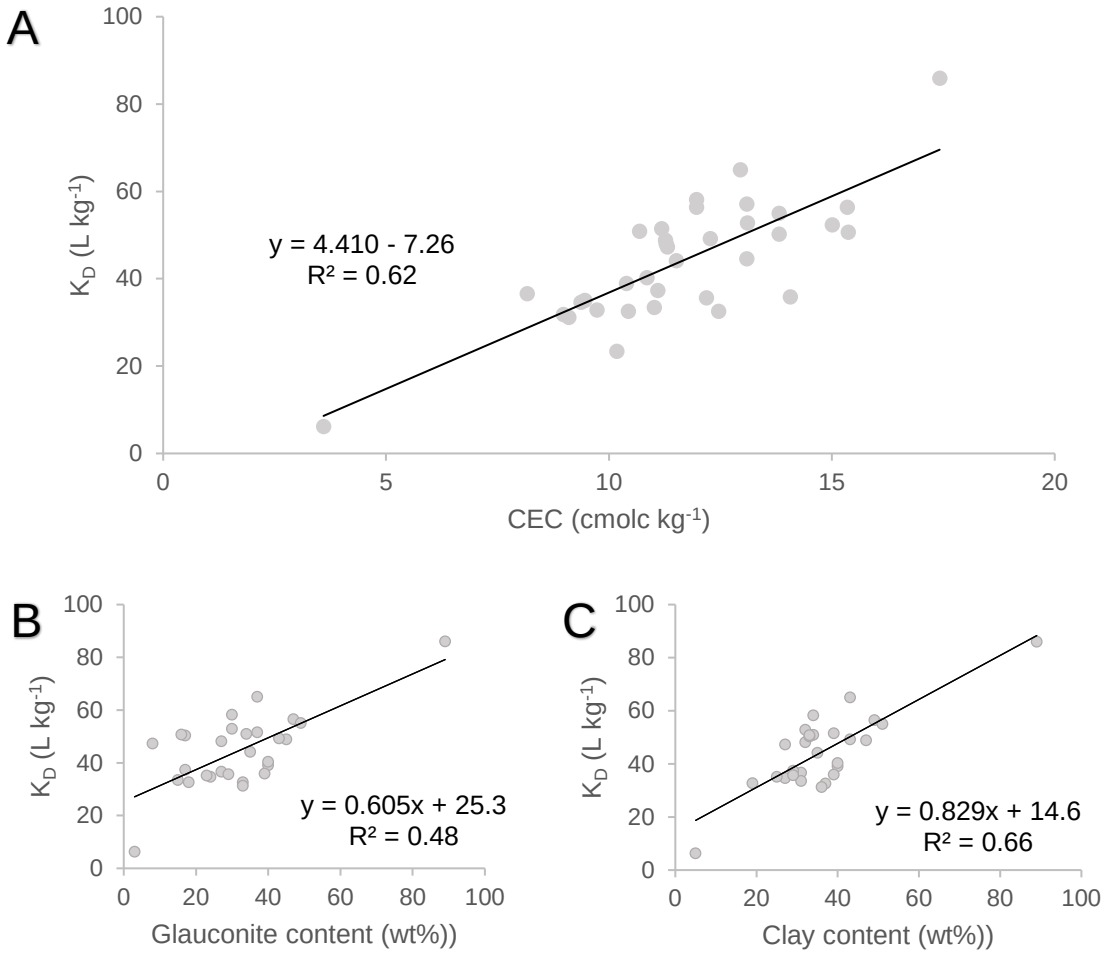


*Figure 2 Linear relationship between the Sr distribution coefficient $K_D$ (L kg$^{-1}$) and the A) cation exchange capacity (CEC – cmol$_c$ kg$^{-1}$), n = 35, complete sands); B) the glauconite content (wt%); and C) the total clay (mineral) content of the complete sand (wt%). The glauconite content by itself gives a poor relation to the $K_D$ of the complete sand ($R^2$ = 0.48).*

Focussing on isolated glauconite from the subsurface samples, a linear relation can be found between the $K_D$ of the glauconite fraction (after 48 h) and the CEC of the glauconite fraction ($R^2$ = 0.62) (Figure 3A). In addition, a markedly strong negative relationship was observed between the $K_D$ and the $d_{060}$ reflection ($R^2$ = 0.57) (Figure 3B). The CEC and $d_{060}$ reflection are negatively correlated as well ($R^2$ = 0.57) (Figure 3C). The iron speciation, expected to be linked with the weathering grade, had no correlation to the subsurface glauconite sand and glauconite fraction parameters.

The glauconite phases in the investigated sands have $d_{060}$ reflections between 1.5144 and 1.5190 Å. This range of reflections clearly distinguished the glauconite from illite (1.499 Å) and nontronite (1.521 Å) and less clearly from montmorillonite (1.50-1.52 Å for respectively dioctahedral and trioctahedral montmorillonite) (Emmerich et al., 2009; Moore and Reynolds, 1997). When $K^+$ is leached from glauconite (e.g. during weathering), the interlayer space increases and becomes accessible to larger (hydrated) cations. By weathering the $d_{060}$ reflection broadens and shifts to lower d-values. The transition of an illitic to smectitic end member goes along with an increase in the planar sites and an increase in the total cation exchange capacity. Glauconite weathering hence increases the sorption of $Sr^{2+}$. The trend observed in the glauconite fraction of the subsurface sands is opposite to the comparison of the subsurface versus the weathered surface samples, where lower CEC and lower $K_D$ values were observed for the weathered samples. That may be related to differences in glauconite content as well and it is of note that the differences

in CEC and $K_D$ between surface and subsurface samples were relatively small. Indeed, multivariate analysis showed that there was no significant difference in either CEC or $K_D$ between weathered surface and subsurface samples after correcting for glauconite content (details not shown).

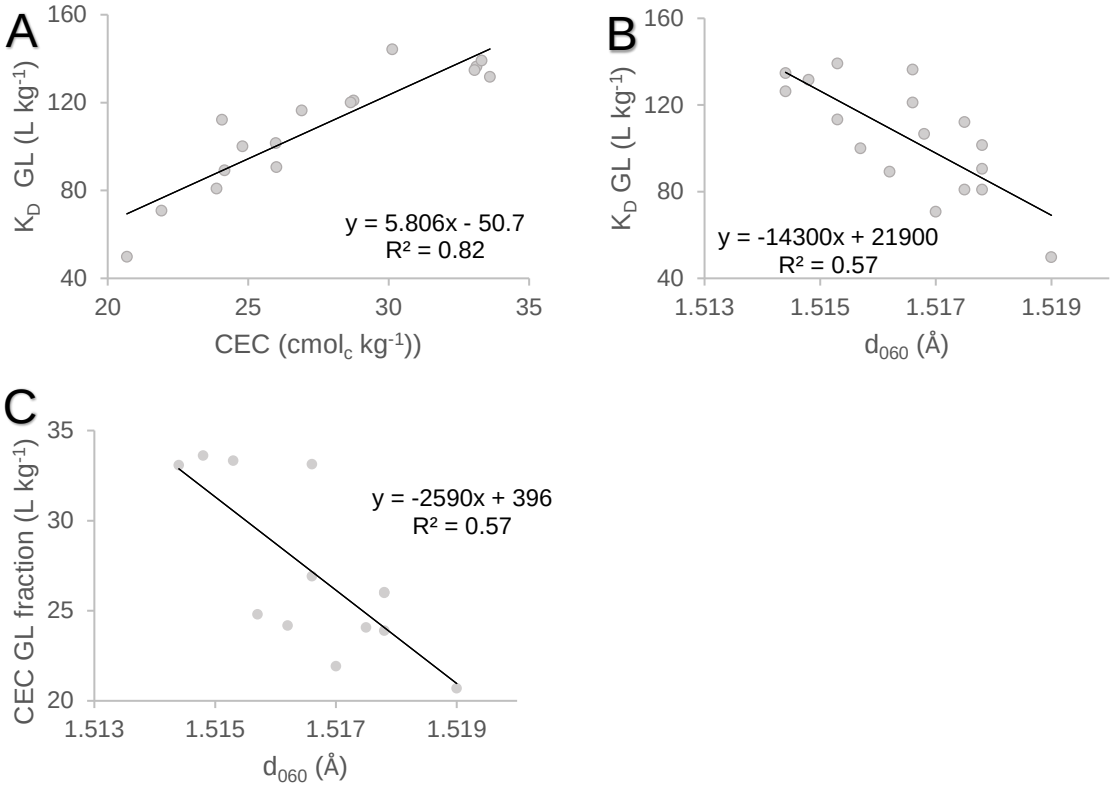


*Figure 3 Linear relationship between the distribution coefficient $K_D$ (L kg$^{-1}$) of the glauconite fraction and A) the CEC of the glauconite fraction ($R^2$ = 0.82); and B) the $d_{060}$ reflection of the clay phase in the XRD pattern ($R^2$ = 0.57) and C) between the CEC of the glauconite fraction and the $d_{060}$ reflection of the clay phase ($R^2$ = 0.57).*

# 4 Discussion

There is a close resemblance in mineralogy between glauconite and (Fe-)illite, apart from the pelletal form in which glauconite mainly occurs. Radiocaesium sorption on the glauconite fraction is in the same range as illite (Bruneel et al., 2020). For $Sr^{2+}$, however, the glauconite fractions have mostly lower $K_D$ values compared to the Illite du Puy reference (50 -144 L $kg^{-1}$ versus 132 L $kg^{-1}$) despite the generally higher CEC values (20.7-33.6 $cmol_C$ $kg^{-1}$ versus 20.4 $cmol_C$ $kg^{-1}$). Hence, $Sr^{2+}$ $K_D$ values per unit of CEC in glauconite are lower compared to illite. The higher CEC can be attributed to the smectitic glauconite layers. Compared to its illitic counterpart, the interlayer space is more accessible for hydrated exchangeable cations, including $Ca^{2+}$ and $Sr^{2+}$. The combination of an increase in the total capacity of sorption sites and a lower $Sr^{2+}$ $K_D$ suggests lower selectivity of $Sr^{2+}$ to $Ca^{2+}$ as well. During weathering of glauconite the number of smectitic layers increases (associated with an increase in CEC and a decrease in $d_{060}$ value). In the subsurface glauconite samples the increase in CEC is associated with an increase in $Sr^{2+}$ $K_D$.

With regard to kinetics, it was observed for radiocaesium that sorption required more time to reach equilibrium than illite (one month versus 48 hours). The sorption sites at the centre of the grain proved to be inaccessible for $Cs^+$. This delay in reaching sorption equilibrium was not seen for Sr sorption, despite the cation being much larger equilibrium is reached within 48 hours. At trace concentration $Cs^+$ sorption will be limited to the FES, while $Sr^{2+}$ sorbs on the planar sites. Caesium can migrate from the FES to the interlayer and exchange for the interlayer $K^+$. This process is much slower, explaining the large differences between the $Cs^+$ and $Sr^{2+}$ sorption kinetics.

The $Sr^{2+}$ $K_D$ values obtained here might be compared with existing models/equations. One way is based on the CEC and the $Ca^{2+}$ concentration in solution (*Eqn. 1*). At trace concentration $Sr^{2+}$, the product of the selectivity coefficient and the fractional $Ca^{2+}$ loading ($K_c$ (Sr/Ca).$Z_{Ca}$) approaches one (Konoplev et al., 1992). Therefore Eqn (1) can be converted to:

$$K_D \approx \frac{CEC}{2\, m_{Ca}} \qquad (3)$$

with units as determined in Eqn. (1). Additionally, several other researchers have determined the correlation between the CEC and Sr $K_D$ values. In Table 5 the experimental data are compared to the calculated $K_D$ values with the method of Konoplev et al. (1992) and Valcke et al. (1998) based on soil data. The calculated $K_D$ values fit markedly strong ($R^2$=) within factors 0.94-1.6 to the experimentally determined values (Table 5).

*Table 5 Comparison of measured and calculated (two ways) $Sr^{2+}$ $K_D$ data for a subset of complete glauconite sands.*

| Formation | Sample | Measured $K_D$ | Calculated $K_D$[$] | Calculated $K_D$[$$] |
|---|---|---|---|---|
| | | L $kg^{-1}$ | L $kg^{-1}$ | L $kg^{-1}$ |
| Diest Fm | D1 | 51 ± 2.4 | 53 | 50 |
| | D2 | 37 ± 11 | 41 | 38 |
| | D3 | 35 ± 3.5 | 47 | 44 |
| | D4 | 35 ± 0.9 | 47 | 44 |
| | D5 | 58 ± 0.1 | 60 | 56 |
| Berchem Fm | B1 | 86 ± 2.0 | 87 | 81 |
| | B2 | 48 ± 4.1 | 56 | 53 |
| | B3 | 33 ± 14 | 55 | 51 |

| | | | | |
|---|---|---|---|---|
| Voort Fm | V1 | 37 ± 7.6 | 56 | 52 |
| | V2 | 47 ± 0.6 | 57 | 53 |
| | V3 | 50 ± 1.1 | 69 | 65 |
| Illite du Puy | Ref | 132 ± 3.2 | 108 | 101 |

*[$] (Konoplev et al., 1992) – $K_c$ = 5 at 0.1 mM $Ca^{2+}$*

*[$$] Linear relation CEC tot $K_D$ determined on soils (Valcke, Cremers et al. 1998) , valid at 4.8 mM $Ca^{2+}$ and multiplied by 4.8 top obtain the value at 1 mM $Ca^{2+}$*

The calculated $K_D$ values, largely based on soil data, slightly overestimate the experimental results, mean ratio of predicted/observed is 1.25 (model Konoplev) or 1.17 (model Valcke and Cremers). The main factors determining the $Sr^{2+}$ $K_D$ are the selectivity coefficient (Sr/Ca) and the $Ca^{2+}$ concentration in solution. Based on Eqn. (1) and the slope of the Kd/CEC correlation, the $K_c$ (Sr/Ca) values should be 0.87.

A note should be made on the CEC analysis as the CEC might be slightly overestimated due to the milling procedure adopted for CEC determination, not for the Sr adsorption. The $Cs^+$ sorption on glauconite sands proved that the internal surface is available for sorption, though it requires longer equilibrium times (Bruneel et al., 2020). As the cobalt (III) hexamine cation complex is much larger than $Ca^{2+}$ and $Sr^{2+}$, we speculated that it is not able to reach all sorption sites that are accessible to $Sr^{2+}$. The CEC values of milled samples (complete sands) are 1.03-2.9 times (mean: 1.7, n=5) higher compared to the corresponding unmilled form data not shown). Milling will open up the mesopores (2-50 nm) and larger pores breaking up the glauconite pellet to a clay sized fraction. The nanopores (< 2 nm) in the particles should remain unaffected. A kinetic experiment showed that the CEC, based on Co adsorption, did not reach equilibrium in 14 days when adopted to the unmilled pellets, the CEC increased with a factor 1.4-2.8 (mean 1.7, n=7) between one hour and 14 days (data not shown), well in contrast with Sr that obtained equilibrium after 48h. Both additional tests suggest that the 1h determined CEC values on the milled samples are probably overestimating the CEC accessible for the Sr exchange on the un-milled samples. With smaller CEC values adopted in the existing models described above, the $K_D$ values would be less overestimated and the $K_c$(Sr/Ca) higher than the value of 0.87, i.e. that uncertainty on CEC may remove the (small) differences between data on glauconite and those on soil.

# 5 Conclusion

The $K_D$ values of $Sr^{2+}$ in the Neogene-Paleogene glauconite sands range from 23 to 65 L $kg^{-1}$ in a 0.5 mM KCl and 1 mM $CaCl_2.H_2O$ background solution. Equilibrium is reached within 48 hours in all fractions (complete glauconite sand, glauconite fraction, milled complete sand and milled glauconite fraction), which means that the glauconite pellets do not limit $Sr^{2+}$ sorption. The internal sorption sites are accessible without time-lag in reaching sorption equilibrium. In the case of a radiostrontium contamination this is an important factor for RN transport, as the glauconite sands are highly permeable.

Pure glauconite fractions show higher sorption with $K_D$ values of 50 to 144 L $kg^{-1}$ in the range of Sr $K_D$ values for illite. The $Sr^{2+}$ sorption $K_D$ of the complete sand is positively correlated with the CEC of the complete sand ($R^2$ = 0.62) and can be predicted very good based on the CEC and Ca concentration. Further, correlation analysis indicated that in the subsurface glauconite sands, Sr sorption on the glauconite sands increase upon weathering due to the formation of more smectite-type layers and associated planar sites. In the investigated range of glauconite fractions, a factor 3 difference in $K_D$ was observed.

# 6 Acknowledgements

This PhD is performed in close cooperation with, and with financial support of ONDRAF/NIRAS, the Belgian Agency for Radioactive Waste and Fissile Materials. We want to thank Pepijn Van Eynde, geologist at the Wienerberger quarry in Rumst for giving us the opportunity to collect samples. The author thanks Rieko Adriaens for showing the outcrops in the Beniksberg, Wijngaardberg and Zavelstraat and providing a set of glauconite fractions that allowed the start of this research.

# 7 Appendix

Part of the samples represented in this paper were studied for $^{137}Cs$ sorption in Bruneel et al. (2020). An overview of the combined $^{137}Cs$ and $^{85}Sr$ sorption data for these 11 samples were given in Table 6.

*Table 6 The log Kd (L kg-1) values of the complete glauconite sands after 35 days, means ± standard deviation of two replicates (Bruneel, Van Laer et al. 2020).*

| | | $^{137}Cs$ sorption | | $^{90}Sr$ sorption | |
|---|---|---|---|---|---|
| Formation | Sample | log $K_D$ (L $kg^{-1}$) complete sand | log $K_D$ (L $kg^{-1}$) glauconite fraction | $K_D$ (L $kg^{-1}$) complete sand | $K_D$ (L $kg^{-1}$) glauconite fraction |
| Diest Fm | D1 | 3.46 ± 0.02 | 4.14 ± 0.03 | 51 ± 2.4 | 116 ± 0.7 |
| | D2 | 3.42 ± 0.03 | 4.16 ± 0.03 | 37 ± 11 | 89 ± 0.1 |
| | D3 | 3.36 ± 0.01 | | 35 ± 3.5 | 121 ± 1.2 |
| | D4 | 3.53 ± 0.01 | | 35 ± 0.9 | 131 ± 0.3 |
| | D5 | 3.75 ± 0.03 | | 58 ± 0.1 | 144 ± 3.6 |
| Berchem Fm | B1 | 4.25 ± 0.05 | 4.27 ± 0.01 | 86 ± 2.0 | 100 ± 3.0 |
| | B2 | 3.59 ± 0.01 | | 48 ± 4.1 | 139 ± 0.3 |
| | B3 | | 4.09 ± 0.02 | 33 ± 14 | |
| Voort Fm | V1 | 3.59 ± 0.02 | | 37 ± 7.6 | 126 ± 0.5 |
| | V2 | 3.57 ± 0.03 | | 47 ± 0.6 | |
| | V3 | 3.86 ± 0.01 | 4.26 ± 0.01 | 50 ± 1.1 | 141 ± 0.7 |
| Illite du Puy | Ref | 4.39 ± 0.05 | | 132 ± 3.2 | |
| Boom Clay | Ref | 3.54 ± 0.03 | | 70 ± 2.3 | |

Results of the t-test (Welch test) assuming unequal variances between the sample groups of weathered (W1-18) versus natural glauconite sand samples (K1, D1-D16, B1-B4, V1-V6) and the glauconite content, CEC, $Sr^{2+}$ $K_D$, $K_c$ (Sr/Ca), the total Fe content and the $Fe^{2+}$ to $Fe_{tot}$ ratio (Table 7).

*Table 7*

| Categorical variable | Continues variable | Test statistics | Probability p | Degrees of freedom |
|---|---|---|---|---|
| Natural versus weathered | Glauconite content | 1.68 | 0.099 | 61.1 |
| | CEC | -2.82 | 0.0065 | 59.9 |
| | $Sr^{2+}$ $K_D$ | -1.75 | 0.084 | 85.4 |
| | $K_c$ (Sr/Ca) | -1.55 | 0.13 | 45.7 |
| | Total Fe content | 3.21 | 0.0051 | 17.3 |
| | $Fe^{2+}$ to $Fe_{tot}$ ratio | -7.11 | <0.0001 | 26.9 |

Optical microscopy of glauconite fractions of subsurface sands show a large variation in grain size, morphology of the glauconite grains and oxidation state. In the surface sands most of the grains are coated with or even fully transformed to iron oxide.

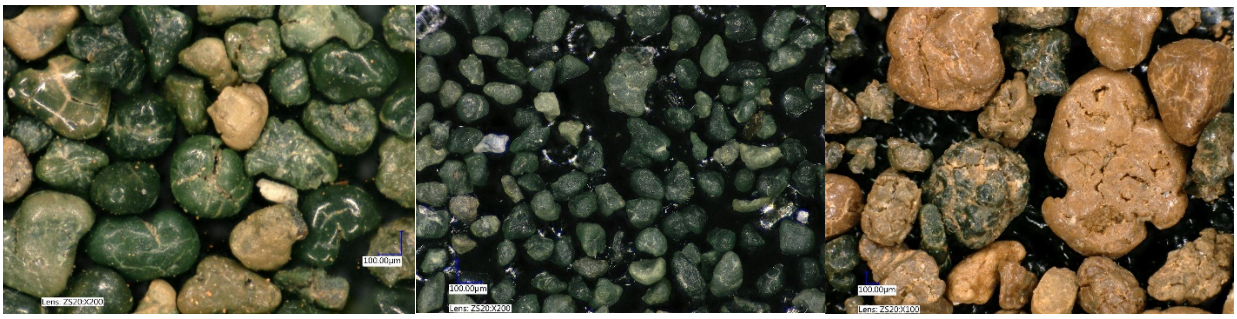

*Figure 4 Optical microscopy of the glauconite fraction of sample D1,V1, W10.*

# 8 References


Adriaens, R., Vandenberghe, N., Elsen, J., 2014. Natural Clay-Sized Glauconite in the Neogene Deposits of the Campine Basin (Belgium). Clay Clay Miner. 62, 35-52.

ALBON, 2009. Afdeling Land en Bodembescherming, Ondergrond & Natuurlijke rijkdommen, Tertiair Geologische kaart Vlaanderen. Vlaamse Overheid, Departemend LNE.

Altmann, S., Aertsens, M., Appelo, T., Bruggeman, C., Gaboreau, S., Glaus, M., Jacquier, P., Kupcik, T., Maes, N., Montoya, V., 2014. Processes of cation migration in clayrocks (CATCLAY), in: Altmann, S., Van Laer, L. (Eds.). Final Scientific Report.

Baeyens, B., Bradbury, M.H., 1995. A Quantitative Mechanistic Description of Ni, Zn and Ca Sorption on Na-Montmorillonite: Part II: Sorption Measurements. Paul Scherrer Insitut (PSI), Würenlingen/Villigen.

Bradbury, M.H., Baeyens, B., 2000. A generalised sorption model for the concentration dependent uptake of caesium by argillaceous rocks. Journal of Contaminant Hydrology 42, 141-163.

Bradbury, M.H., Baeyens, B., 2005. Experimental and Modelling Investigations on Na-Illite: Acid-Base Behaviour and the Sorption of Strontium, Nickel, Europium and Uranyl. Paul Scherrer Institut (PSI), Villigen.

Brouwer, E., Baeyens, B., Maes, A., Cremers, A., 1982. Cesium Ion Equilibria Illite Clay Abstr. Pap. Am. Chem. Soc. 183, 97-COLL.

Bruneel, Y., Van Laer, L., Brassinnes, S., Smolders, E., 2020. Radiocaesium sorption on natural glauconite sands is unexpectedly as strong as on Boom Clay. Sci. Total Environment 720, 137392.

Courbe, C., Velde, B., Meunier, A., 1981. Weathering of glauconites: reversal of the glauconitization process in a soil profile in western France. Clay Miner. 16, 231-243.

Cremer, M., Schlocker, J., 1976. Lithium borate decomposition of rocks, minerals, and ores. American Mineralogist 61, 318-321.

Emmerich, K., Wolters, F., Kahr, G., Lagaly, G., 2009. Clay profiling: The classification of montmorillonites. Clay Clay Miner. 57, 104-114.

Fuller, A.J., Shaw, S., Peacock, C.L., Trivedi, D., Small, J.S., Abrahamsen, L.G., Burke, I.T., 2014. Ionic strength and pH dependent multi-site sorption of Cs onto a micaceous aquifer sediment. App. Geochem. 40, 32-42.

Konoplev, A., Bulgakov, A., Popov, V., Bobovnikova, T.I., 1992. Behaviour of long-lived Chernobyl radionuclides in a soil–water system. Analyst 117, 1041-1047.

Louwye, S., De Coninck, J., & Verniers, J. , 1999. Dinoflagellate cyst stratigraphy and depositional history of Miocene and Lower Pliocene formations in northern Belgium (southern North Sea Basin). Geologie en Mijnbouw 78.1, 31-46.

Louwye, S., De Schepper, S., 2010. The Miocene–Pliocene hiatus in the southern North Sea Basin (northern Belgium) revealed by dinoflagellate cysts. Geological Magazine 147, 760-776.

Louwye, S., De Schepper, S., Laga, P., Vandenberghe, N., 2006. The Upper Miocene of the southern North Sea Basin (northern Belgium): a palaeoenvironmental and stratigraphical reconstruction using dinoflagellate cysts. Geological Magazine 144, 33.

Meunier, A., 2005. Clays. Springer Science & Business Media.

Meunier, A., El Albani, A., 2007. The glauconite?Fe-illite?Fe-smectite problem: a critical review. Terra Nova 19, 95-104.

Missana, T., Benedicto, A., García-Gutiérrez, M., Alonso, U., 2014. Modeling cesium retention onto Na-, K- and Ca-smectite: Effects of ionic strength, exchange and competing cations on the determination of selectivity coefficients. Geochimica et Cosmochimica Acta 128, 266-277.

Moore, D.M., Reynolds, R.C., 1997. X-ray diffraction and the identification and analysis of clay minerals, 2nd ed. ed. Oxford : Oxford university press.

Poinssot, C., Baeyens, B., Bradbury, M.H., 1999. Experimental Studies of Cs, Sr, Ni and Eu Sorption on Na-illite and the Modelling of Cs Sorption. Paul Scherrer Institut (PSI), Villigen.

Suhr, N.H., Ingamells, C.O., 1966. Solution Technique for the Analysis of Silicates. Analytical Chemistry 38, 730-734.

Valcke, E., Cremers, A., Moskaltchuk, L., 1998. The use of sapropels as amendments in radiocaesium and radiostrontium contaminated soils. App. Geochem. 13, 155-164.

Van Ranst, E., De Coninck, F., 1983. Evolution of glauconite in imperfectly drained sandy soils of the Belgian Campine. Journal of Plant Nutrition and Soil Science 146, 415-426.

Vandenberghe, N., Van Simaeys, S., Steurbaut, E., Jagt, J. W. M., & Felder, P. J., 2004. Stratigraphic architecture of the Upper Cretaceous and Cenozoic along the southern border of the North Sea Basin in Belgium. Netherlands Journal of Geosciences 83, 155-171.

Voronina, A.V., Blinova, M.O., Semenishchev, V.S., Gupta, D.K., 2015. Returning land contaminated as a result of radiation accidents to farming use. J Environ Radioact 144, 103-112.

Wallace, S.H., Shaw, S., Morris, K., Small, J.S., Fuller, A.J., Burke, I.T., 2012. Effect of groundwater pH and ionic strength on strontium sorption in aquifer sediments: Implications for 90Sr mobility at contaminated nuclear sites. App. Geochem. 27, 1482-1491.